The International Journal of Engineering and Science (IJES)
|| Volume || 13 || Issue || 10 || Pages || PP 96-103 || 2024 ||
ISSN (e): 2319 – 1813 ISSN (p): 2319 – 1805

Numerical Prediction of Pressure Oscillation in a Centrifugal Pump at Shut-off conditions

Di Yu[1], Xu-Lai Chen[1], Fu-Yi Zhang[2], He-Chao Guo[2], Zhi-Yang Zhao[2] , Shen Chen[2]

1. Zhejiang Testing & Inspection Institute for Mechanical and Electrical Products Quality Co.,Ltd., Hangzhou, 311305, China

2. College of Mechanical Engineering, Quzhou University, Quzhou, 324000, China

Abstract: *In order to investigate the pressure fluctuation characteristics of centrifugal pumps under shut-off conditions, a numerical calculation was carried out using Fluent software based on the RNG k-ε turbulence model. The pressure fluctuation characteristics within the volute and impeller flow fields of the centrifugal pump under shut-off conditions were analyzed, and the shut-off head was predicted. The results show that the monitoring points within the volute flow passage exhibit obvious periodic patterns, and their peak pressure fluctuations occur at frequencies that are multiples of the vane passing frequency. Additionally, the closer the monitoring point is to the volute tongue, the greater the amplitude of pressure fluctuation. Furthermore, for monitoring points located on the centerline of the impeller flow passage, the closer they are to the impeller exit, the greater the amplitude of pressure fluctuation.*

Keywords: *Centrifugal Pump; Shut-Off Point; Pressure Fluctuation; Transient*

Date of Submission: 11-10-2024 Date of acceptance: 22-10-2024

I. Introduction

Historically, the hydraulic design of centrifugal pumps did not explicitly require performance specifications at the shut-off point. However, with the rapid development of the social economy, specific types of centrifugal pumps now have explicit requirements for shut-off point performance. For instance, in the renewable energy sector, pumps used in wind power generation and solar water heating systems need to meet higher shut-off point performance standards to ensure normal operation under low flow conditions. Similarly, shipboard pumps and nuclear power pumps must possess excellent shut-off point performance to adapt to complex working environments and high safety standards.

The current research on the shut-off point of centrifugal pumps primarily focuses on the calculation of shut-off head. Stepanoff corrected and calculated the shut-off head of centrifugal pumps at zero flow rate by modifying the expression of Euler's equation, and based on the statistical analysis of experimental data, a constant correction coefficient was provided [1]. Frost et al. theoretically derived the calculation expressions for the shut-off head of impeller and volute [2]. Liu Houlin et al. performed practical calculations and comparisons on 34 centrifugal pumps, analyzed the accuracy and applicable ranges of various calculation methods, and carried out fluid-structure interaction numerical calculations on the structural field under shut-off conditions [3–5]. The results showed that the displacement deformation and equivalent stress in the area near the tongue between the front and rear cover plates of the impeller were the largest; the displacement deformation of each blade gradually increased from inlet to outlet, but the maximum equivalent stress of each blade was not at the blade exit edge. Yuan Shouqi et al. used wavelet packets to decompose the pressure signal of the centrifugal pump and established characteristic signals in different frequency ranges [6]. The results indicated that the pressure pulsation at the shut-off point of the centrifugal pump exhibited irregular changes without obvious periodicity, and low-frequency pulsations below one times the blade passing frequency dominated. Zhang Yuliang, Wang Yong, etc., both numerically simulated the internal flow field of low specific speed centrifugal pumps during rapid valve closure startup processes [7, 8]. The results showed that with the continuous increase of speed during startup, the dynamic-static interference effect becomes more pronounced; a shock head appeared at the end of the startup process under different acceleration conditions.

For the study of pressure pulsation characteristics in unsteady flow fields within pumps, there are mainly two approaches: experimental research and numerical computation. In terms of experimental research, many scholars at home and abroad have conducted relevant studies. Zhang Yuliang et al. collected pressure pulsation data at the volute wall of a centrifugal pump using pressure sensors and analyzed the amplitude and

intensity of pressure pulsations under different rotational speed conditions [9]. They found that the intensity of pressure pulsations was significant at the volute exit. Tan Linwei et al. obtained time-frequency domain diagrams of pressure pulsations within the pump under different rotational speed conditions using high-frequency pressure sensors [10]. The results indicated that as the rotational speed increased, the interference between the impeller and volute intensified, and the periodicity of pressure pulsations became more pronounced. Jiang Wei et al. investigated the influence of semi-high guide vanes on the pressure pulsation characteristics within a centrifugal pump [11]. It was found that reducing the height of the guide vanes could significantly decrease the amplitude of pressure pulsations at the cutwater and downstream locations. Xiao Yexiang et al. focused on the impact of rotating stall on pressure pulsations [12]. They discovered that the interaction between the stalled cells and the cutwater might lead to rotor-stator interactions. Wang Chunlin et al. conducted a numerical simulation study on the vibration and noise of a double-suction centrifugal pump [13]. They found that the pressure pulsations at the cutwater were the primary noise source and resonated with the volute. Chen Jie et al. used three-dimensional numerical simulation to analyze the internal flow field, radial forces on the impeller, and pressure pulsations across various sections of the volute in a ultra-low specific speed centrifugal pump with a specific speed of n_s=25 [14]. The results showed that the coupling effect between the impeller exit and the volute was the main influencing factor for pressure pulsations within the volute.

In summary, most current studies on pressure pulsations in centrifugal pumps focus on design conditions, while research on pressure pulsations under shut-off conditions is scarce. Based on this, this paper investigates the pressure pulsation characteristics of a centrifugal pump model under shut-off conditions, predicts the head variation under these conditions, and also deeply explores the internal flow characteristics of the centrifugal pump under shut-off conditions.

II. Computational Model and Methodology

2.1 Computational Model

The three-dimensional model of the centrifugal pump is shown in Figure 1. Its rated parameters are as follows: flow rate Q = 100 m³/h, head H = 124 m, and rotational speed n = 2900 rpm. Additionally, the pump inlet diameter D_1 = 100 mm, pump outlet diameter D_2 = 65 mm, impeller outer diameter D_3 = 320 mm, and impeller outlet width b_2 = 12 mm.

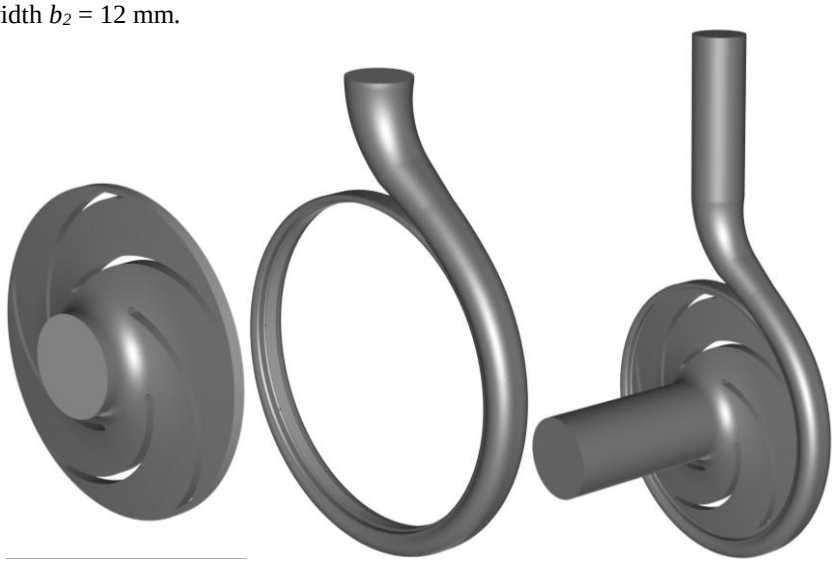

(a) Impeller (b)Volute (c)Overall Model

Figure 1 Three-Dimensional Model of Centrifugal Pump (a) Impeller (b) Volute (c) Overall Model

The meshing of the centrifugal pump was performed using ICEM CFD 19.2. The grids for the impeller, volute, and the overall centrifugal pump are shown in Figure 2, with a total of 1,032,286 grids for the entire pump. Specifically, the number of grids for the impeller, volute, inlet pipeline, and outlet pipeline are 533,164, 297,788, 106,856, and 94,478, respectively.

(a) Impeller (b)Volute (c)Overall Model

Figure 2 Meshing of the Centrifugal Pump (a) Impeller (b) Volute (c) Overall Model

2.2 Governing Equations

Existing literature has confirmed that the RNG *k-ε* model can achieve good computational results for pressure pulsation calculations in pumps [15, 16]. Therefore, this paper selects the RNG *k-ε* two-equation model to close the Reynolds-averaged equations for unsteady turbulent flow calculations. The RNG *k-ε* model is an improved version of the Standard k-ε model. Compared to the Standard *k-ε* model, the RNG *k-ε* model introduces the time-averaged strain rate of the main flow, increasing the influence of the mean strain rate. Additionally, the turbulence generation and turbulent kinetic energy dissipation equations in this model are the same as those in the standard *k-ε* model, with only modifications made to the constant terms. Thus, for unsteady, incompressible flows, the turbulent kinetic energy dissipation equation is transformed into:

$$\frac{\partial\left(\rho U_j \varepsilon\right)}{\partial x_j}=\frac{\partial}{\partial x_j}\left[\left(\mu+\frac{\mu_t}{\sigma_{\varepsilon\mathrm{RNG}}}\right)\frac{\partial \varepsilon}{\partial x_j}\right]+\frac{\varepsilon}{\kappa}\left(C_{\varepsilon 1\mathrm{RNG}}P_\kappa-C_{\varepsilon 2\mathrm{RNG}}\rho\varepsilon+C_{\varepsilon 1\mathrm{RNG}}P_{\varepsilon b}\right) \quad (1)$$

where: $\sigma_{\varepsilon\mathrm{RNG}}=0.7179$; $C_{\varepsilon 1RNG}=1.42-f_\eta$; $C_{\varepsilon 2RNG}=1.68$; the equation coefficient f_η is expressed as:

$$f_\eta=\frac{\eta\left(1-\frac{\eta}{4.38}\right)}{\left(1+\beta_{\mathrm{RNG}}\eta^3\right)} \quad (2)$$

Where: $\beta_{\mathrm{RNG}}=0.012$; The equation coefficient η is expressed as:

$$\eta=\sqrt{\frac{P_\kappa}{\rho C_{\mu\mathrm{RNG}}\varepsilon}} \quad (3)$$

2.3 Numerical Scheme

To investigate the characteristics of pressure pulsations within a centrifugal pump under deadhead conditions, numerical calculations were conducted using Ansys Fluent software. Considering the viscous effects, no-slip boundary conditions were applied at the walls. The coupling of velocity and pressure was achieved using the SIMPLE algorithm, and default under-relaxation factors were used for all variables during iterative calculations. For this computation, the total time was set to the duration required for the impeller to rotate 10 times. Given that the rated speed of the pump is 2900 rpm, the time taken for the impeller to rotate 1° is 0.0000575 seconds. Consequently, the final time step was determined to be 0.0000575 seconds, resulting in a total duration of 0.207 seconds. A maximum of 50 iterations was set for each time step to ensure absolute convergence within each time step, with a residual convergence criterion of 0.001.

III. Results Analysis

3.1 Shutoff Head Prediction

Figure 3 depicts the shutoff head prediction curve for the centrifugal pump at the 10th rotation cycle. As shown in the figure, the shutoff head curve exhibits five peaks and five troughs, with unequal amplitudes across these peaks and troughs. The differences between successive peaks and troughs are 34.21, 35.45, 37.14, 35.7, and 35.38 meters respectively, indicating a trend of initial increase followed by a decrease. Additionally, the number of peaks and troughs corresponds to the number of impeller blades, suggesting that the dynamic interaction between the blades and the volute tongue significantly influences the shutoff head pulsations.

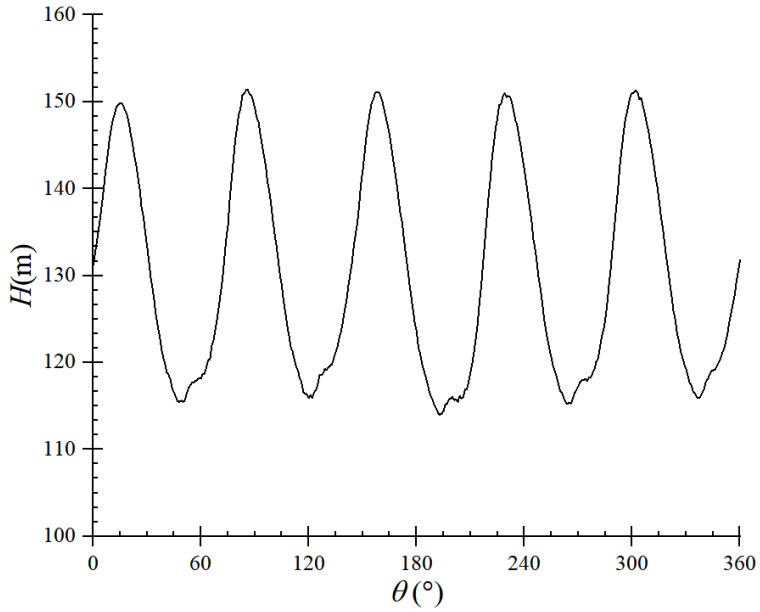

Figure 3 Head Pulsation Curve

3.2 Internal Flow Analysis

To provide a detailed analysis of how the flow field within the pump changes over time, four specific moments when Passage 1 sweeps past the tongue are selected for examination. The relative position angle between the blade and the tongue is denoted by the phase angle θ, with θ=0° representing the moment when the blade is directly facing the tongue. Since the pump has 5 blades, the four moments correspond to the following angles: θ=0°, θ=18°, θ=36°, and θ=54°.

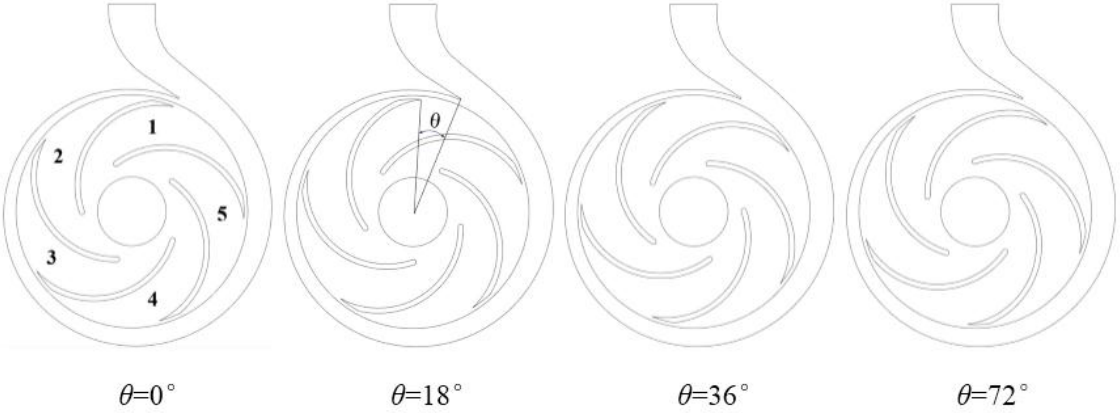

Figure 4 Blade Position

Figure 5 illustrates the static pressure distribution at various time points within the pump during the shutoff condition. As observed from the figure, there is minimal change in the overall static pressure distribution as the impeller rotates. However, the high-pressure area at the outlet side of the working surface of Passage 1 continues to expand with the rotation of the impeller. At 36° rotation of the passage, under the influence of the tongue, this high-pressure area rapidly enlarges and spreads to the outlet section of the pump, reaching a value of 1,500,000 Pa. In the volute flow region, the pressure values between cross-sections I and IV are relatively

lower compared to other locations, which is due to these positions being farther away from the pump's tongue. For the pump's outlet section, the static pressure values are notably higher than those in other parts of the pump, especially evident when Passage 1 rotates by 36°.

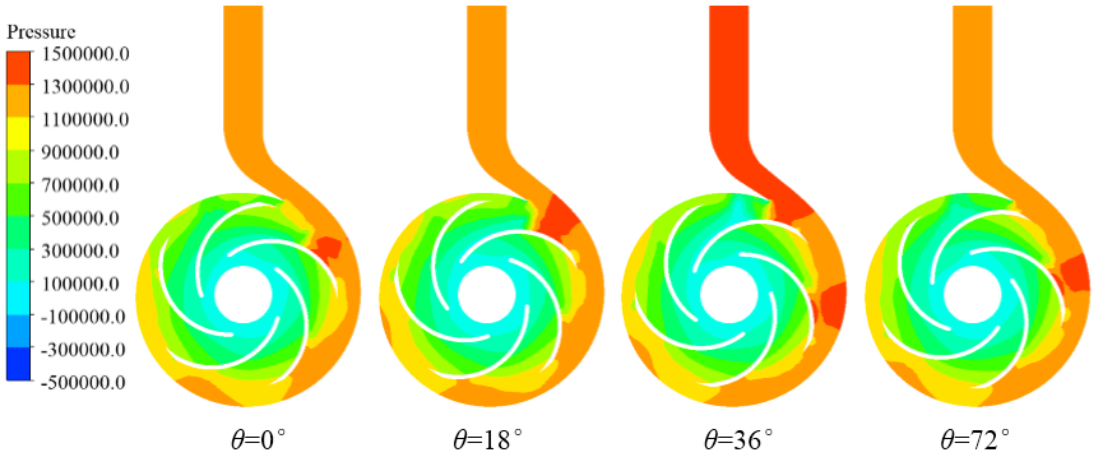

Figure 5 Static Pressure Distribution at Mid-Section in Pump (Pa)

Figure 6 displays the relative velocity contours and streamlines on the impeller mid-plane under the shutoff condition. It is evident from the figure that, at all times, the impeller channels exhibit a varying number of vortices with different shapes and sizes. These vortices are present almost throughout the entire impeller channels, indicating severe rotating stall within the pump under shutoff condition. At the θ=0° instant, except for Passage 5, each impeller channel contains only one vortex occupying the entire flow region. In contrast, at the exit of Passage 5, a larger vortex gives birth to a smaller one. As the impeller rotates to θ=18°, θ=36°, and θ=54°, under the influence of the volute tongue, the vortex at the exit of Passage 1 gradually separates into two vortex centers, generating a smaller vortex, while the remaining passages each have only one vortex filling the entire channel. Regarding the relative flow velocities in the impeller region, it can be observed that, due to the effect of the blades, the velocity within the impeller channels increases progressively towards the impeller exit, reaching a maximum of 50 m/s at the exit. Furthermore, the velocity is greater closer to the volute tongue location.

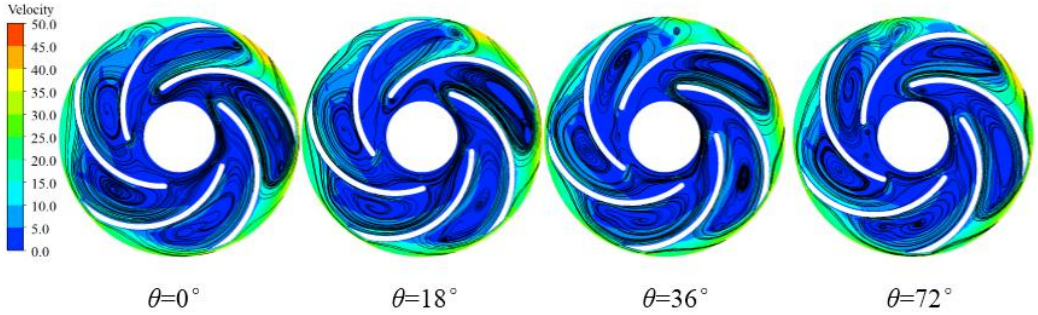

Figure 6 Relative Velocity Distribution on Impeller Mid-Plane (m/s)

3.3 Analysis of Pressure Fluctuations

To investigate the unsteady pressure pulsation within the pump under shutoff conditions, eight monitoring points ($P_{1\text{-}8}$) were strategically placed across cross-sections I to VIII of the volute, along with three additional monitoring points (P_9, P_{10}, and P_{11}) located on the central line of Passage 1 of the impeller. The specific distribution of these monitoring points is illustrated in Figure 7.

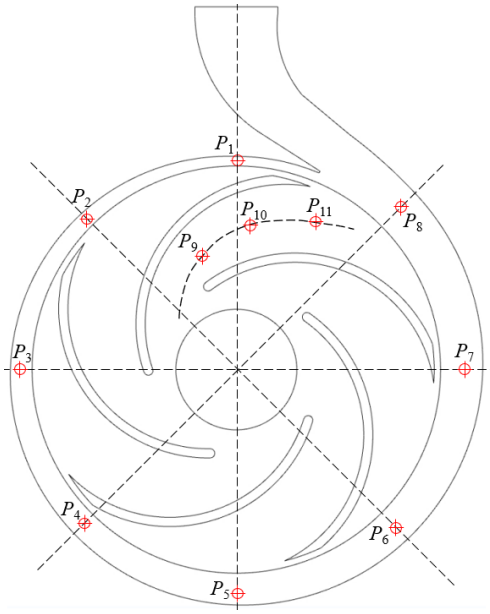

Figure 7 Schematic of Monitoring Point Locations in the Pump

During the unsteady calculation process, a simulation of 10 impeller rotations was conducted. However, at the beginning of the computation, the flow field inside the pump was unstable. To reduce errors, this paper only selects data from the final rotation of the impeller for analysis. Figure 8(a) shows the time-domain plots of pressure fluctuations at the eight monitoring points ($P_{1–8}$) across the volute sections, and Table 1 lists the amplitudes of pressure fluctuations at each monitoring point. From the figure, it can be seen that the pressure fluctuation variations at each volute section exhibit distinct periodic patterns, with each monitoring point having five peaks and valleys within the cycle. The amplitude of pressure fluctuations varies among the monitoring points at different section locations within the volute. Since the monitoring points $P_{3–6}$ are located at sections farther away from the volute tongue, their pressure fluctuation amplitudes are relatively small, with values of 155.3042, 116.3327, 138.619, and 102.616 kPa, respectively. The pressure fluctuation at the monitoring point P_1, which is close to the volute tongue, is significantly large, with an amplitude of 590.3888 kPa. Next are the monitoring points P_8, P_7, and P_2, with corresponding pressure fluctuation amplitudes of 255.468, 236.504, and 233.321 kPa, respectively. For a clearer comparison of the relationship between the magnitude and frequency of pressure fluctuations at the monitoring points, Fast Fourier Transform (FFT) was applied to the pressure fluctuation signals to obtain the corresponding frequency domain plots. As shown in Figure 8(b), high-amplitude pressure fluctuations at each monitoring point occur primarily at low multiple frequencies of the blade passing frequency. The peak values at the first harmonic of the blade passing frequency are the largest, with values of 213.389, 80.011, 63.492, 46.571, 63.226, 44.846, 124.796, and 104.969 kPa, respectively. It can be observed that the closer the monitoring points are to the volute tongue, the greater the amplitude of pressure fluctuations, influenced by the dynamic interaction between the blades and the volute tongue. In summary, for the monitoring points at the volute sections, high-amplitude pressure fluctuations mainly occur at multiples of the blade passing frequency. Higher peak values are found near Sections I, VII, and VIII.

Table 1 Amplitudes of Pressure Fluctuations at Monitoring Points on Volute Sections

Monitoring Point	P_1	P_2	P_3	P_4	P_5	P_6	P_7	P_8
Amplitude (kPa)	590.388	233.321	155.304	116.332	138.619	102.616	255.468	236.504

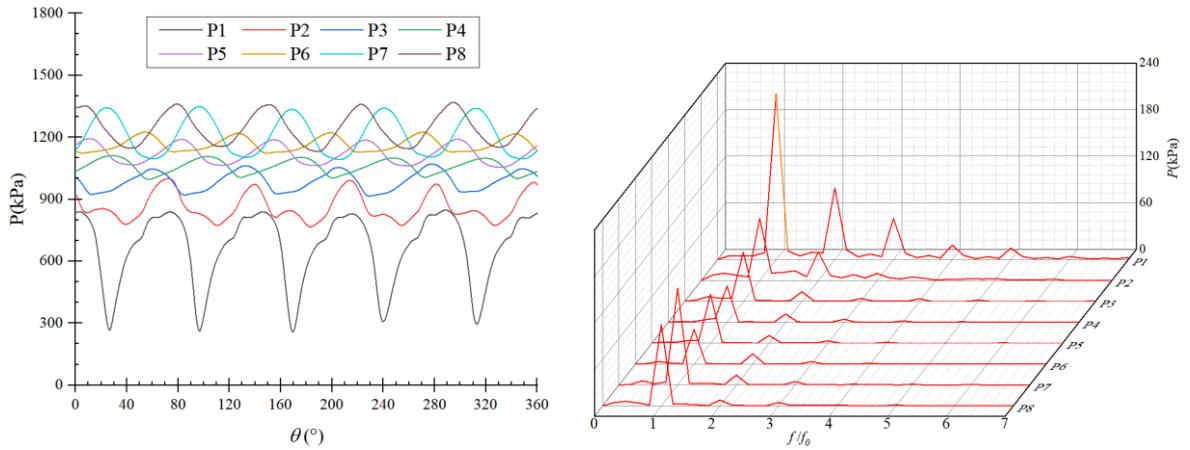

(a) Time-Domain Plot (b) Frequency-Domain Plot

Figure 8 Pressure Fluctuation at Monitoring Points in the Volute (a) Time-Domain Plot (b) Frequency-Domain Plot

Figure 9(a) shows the time-domain plots of pressure fluctuations at monitoring points $P_{9–11}$ on the central line of impeller channel 1, and Table 2 lists the corresponding pressure fluctuation amplitudes at these monitoring points. From the graph, it can be observed that the time-domain curves at each monitoring point exhibit significantly different trends, all showing a pattern of initial decrease, followed by increase, and then decrease again. The reason for this trend is that when the impeller channel 1 rotates by 48 degrees, its outlet aligns directly with the volute tongue position, resulting in lower pressure values at the monitoring points on this central line. As the impeller continues to rotate, the pressure values gradually increase until the trailing edge of the impeller channel 1's blade aligns with the volute tongue. At the same moment, monitoring points closer to the impeller exit experience higher pressure values due to the influence of exit recirculation and the dynamic interaction between the moving and stationary components, leading to larger pressure fluctuation amplitudes. Additionally, the pressure fluctuation amplitudes at monitoring points $P_{9–11}$ are 125.945, 277.981, and 411.098 kPa, respectively, following the pattern where pressure fluctuation amplitudes increase as they get closer to the impeller exit. Figure 9(b) displays the frequency-domain plots of pressure fluctuations at the monitoring points on the central line of impeller channel 1. It can be seen that the pressure at these monitoring points decreases monotonically with increasing frequency, reaching the maximum peak at 0.2 times the blade passing frequency, with values of 24.801, 81.913, and 134.222 kPa, respectively.

Table 2 Amplitudes of Pressure Fluctuations at Monitoring Points on the Central Line of Impeller Channel 1

Monitoring Point	P_9	P_{10}	P_{11}
Amplitude (kPa)	125.945	277.981	411.098

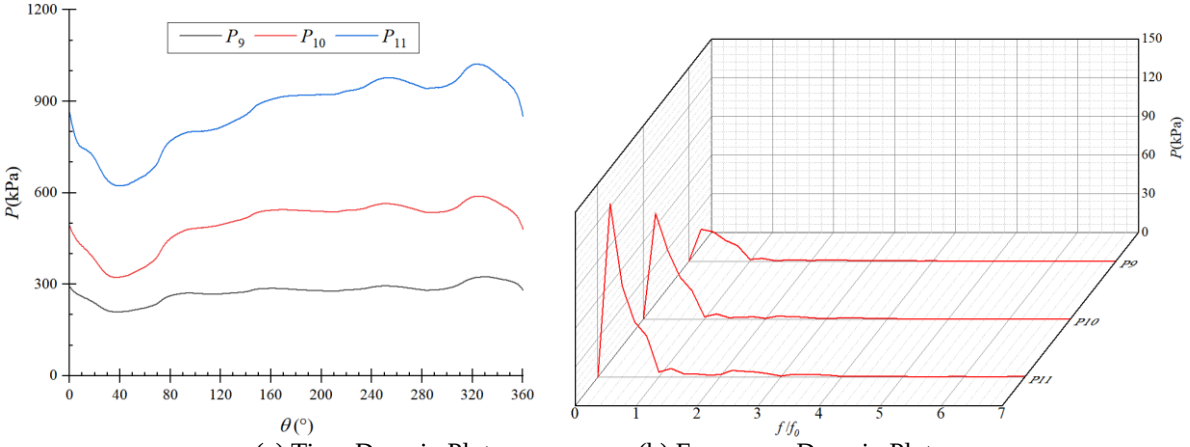

(a) Time-Domain Plot (b) Frequency-Domain Plot

Figure 9 Pressure Fluctuation at Monitoring Points on the Central Line of Impeller Channel 1 (a) Time-Domain Plot (b) Frequency-Domain Plot

IV. Conclusions

(1) The shutoff head curve of the pump exhibits five peaks and five troughs, with unequal amplitudes among the peaks and troughs.

(2) For monitoring points at the volute cross-sections, high-amplitude pressure fluctuations occur at the multiples of the blade passing frequency; notably higher peaks are observed near cross-sections I, VII, and VIII.

(3) The time-domain curves at the impeller channel monitoring points show a trend of initial decrease, followed by an increase, and then a decrease again. Moreover, the pressure fluctuation amplitude increases as one moves closer to the impeller exit.

References

[1]. Dyson G. A review of closed valve head prediction methods for centrifugal pumps[J]. Proceedings of the Institution of Mechanical Engineers, Part A: Journal of Power and Energy, 2002, 216(4): 329–337.

[2]. Frost T H, Nilsen E. Shut–off head of centrifugal pumps and fans[J]. Proceedings of the Institution of Mechanical Engineers, Part A: Journal of Power and Energy, 1991, 205(3): 217–223

[3]. Liu Houlin, Wu Xianfang, Tan Minggao. Head calculation and amendments for centrifugal pumps at shut off condition[J]. Transactions of the CSAE, 2011, 27(9): 43–47.

[4]. WU Xian-fang, LIU Hou-lin, DENG Bang-hua, et al. An Analysis of the Impeller Structure Field of a Centrifugal Pump at Shut-off Condition[J]. China Rural Water and Hydropower, 2015(10): 136140.

[5]. WU Xian-fang, TAN Ming-gao, LIU Hou-lin, et al. A Test of Flow Induced Vibration in a Centrifugal Pump under Shut off Conditions[J]. China Rural Water and Hydropower, 2015(1): 176–179.

[6]. Yuan Shouqi, Huang Ping, Luo Yin, et al. Flow analysis based on wavelet packet decomposition for centrifugal pumps at shut-off condition[J]. Journal of Drainage and Irrigation Machinery Engineering, 2011, 29(4): 282–286.

[7]. ZHANG Yu-liang, ZHU Zu-chao, LIN Hui-chao, et al. Numerical Simulation of Unsteady Flow in Centrifugal Pump During Startup Period at Shut-Off Condition[J]. CHINESE QUARTERLY OF MECHANICS, 2012, 33(3): 436–442.

[8]. Wang Yong, Chen Jie, Liu Houlin, et al. Transient characteristic analysis of ultra-low specific-speed centrifugal pumps during startup period under shut-off condition[J]. Transactions of the Chinese Society of Agricultural Engineering, 2017, 33(11): 68–74.

[9]. Zhang Yuliang, Li Jinfu, Wang Tao, et al. Pressure distribution on the inner wall of the volute casing of a centrifugal pump[J]. Science and Technology of Nuclear Installations, 2022, 2022: 3563459.

[10]. TAN Linwei, NIU Guoping, SHI Weidong, et al. Experimental Investigation of Pressure Fluctuations for Centrifugal Pumps at Different Rotational Speed[J]. Journal of Nantong University (Natural Science Edition), 2020, 19(2): 56–63.

[11]. JIANG Wei，ZHU Xiangyuan, TIAN Hui, et al. Numerical and experimental study of influence of semi-high guide vane on pressure fluctuation in centrifugal pump[J]. Journal of Central South University (Science and Technology), 2021, 52(4): 1276–1286.

[12]. Zhao Xiaoran, Xiao Yexiang, Wang Zhengwei, et al. Unsteady flow and pressure pulsation characteristics analysis of rotating stall in centrifugal pumps under off-design conditions[J]. Journal of Fluids Engineering, 2018, 140(2): 021105.

[13]. Wang Chunlin, Zeng Cheng, Yang Xiaoyong, et al. Numerical simulation and performance prediction of positive and negative internal flow field of double suction pump[J]. Journal of Drainage and Irrigation Machinery Engineering, 2015, 33(07): 577–582.

[14]. Chen Jie, Wang Yong, Liu Houlin, et al. Internal flow and unsteady characteristics of ultra–low specific speed centrifugal pump[J]. Journal of drainage and irrigation machinery engineering, 2018, 36(5): 377–383.